## Supplemental figures

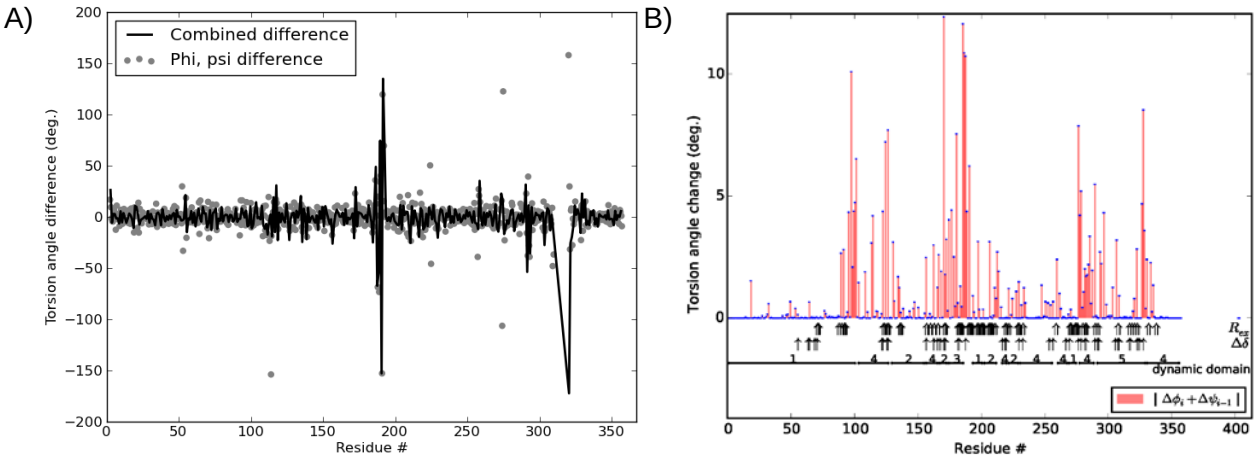


*Figure S1: Torsion angle differences between substrate-bound and –free structures of arginine kinase. (A) Differences in φ and ψ, and in the combined* $\Delta\theta_i = \Delta\psi_{i-1} + \Delta\phi_i$ *for the two unmodified structures are plotted vs. residue number; (B) Pseudo-torsion angles have been refined for the substrate-bound form to superimpose upon the substrate-free form, using an* $\ell^1$*-Norm restraint weight λ=2 (see Experimental Procedures). Residues are annotated by the dynamic domain rigid-group designation (Hayward and Lee, 2002; Niu et al., 2011), observation of NMR relaxation exchange ($R_{ex}$) in the substrate-free (Davulcu et al., 2009) or –bound (this work) states, or significant NMR chemical shift perturbation (Δδ) between substrate-free and -bound forms, the latter excluding amino acids in close proximity to substrates.*

A)

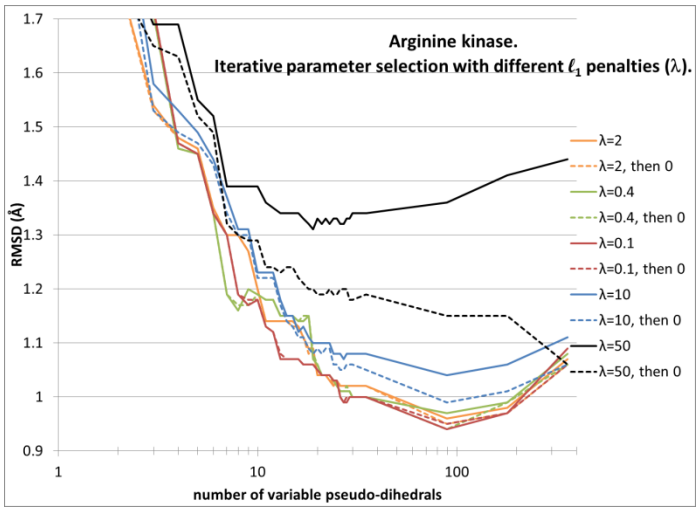


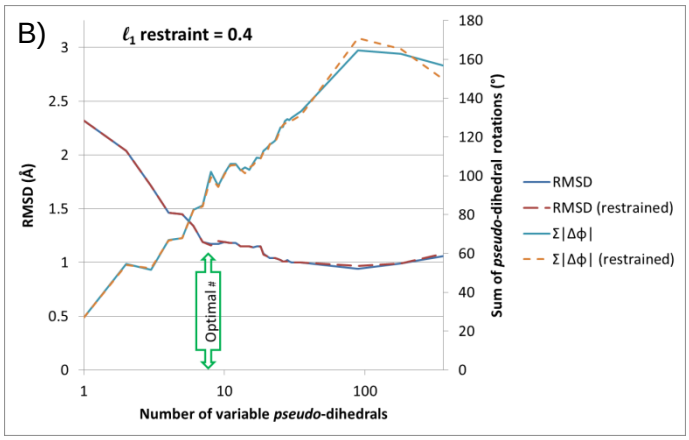


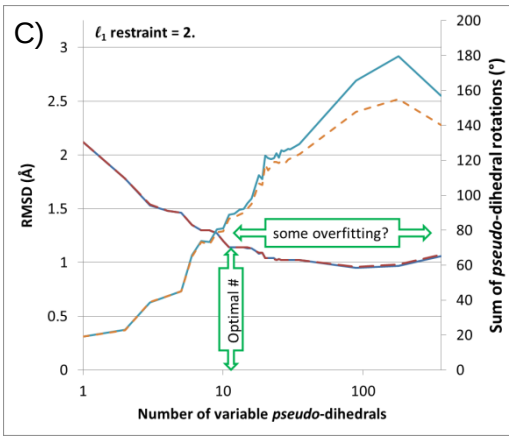


D)

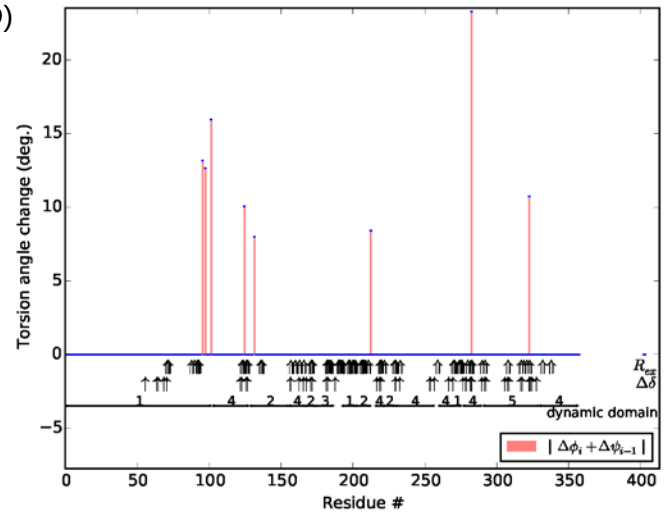


*Figure S2: Subset selection of the most consequential torsion angles. (A-C) Each point*

*represents a refinement from the AK TSA structure to superimpose on the substrate-free form (backbone + $C_\beta$). The RMSD is shown following 20 cycles with an $\ell^1$ restraint (solid lines), and also after 20 additional cycles of unrestrained refinement (dotted) (see Experimental Procedures). Moving from right to left, refinements were re-started with successively fewer variable torsion angles, selecting the pseudo-dihedrals of the previous $\ell^1$-restrained batch that had changed most. (A) Refinement sets with varying weight on the $\ell^1$ restraint, $0.1 \leq \lambda \leq 50$. (B) At λ = 0.4, the $\ell^1$-norm has negligible effect on pseudo-dihedrals. (C) At λ = 2.0, the $\ell^1$-norm is beginning to impact the total dihedral rotation. (D) Selected with λ = 0.4, the top 8 dihedrals (and those selected with different λ,Table S2) approximate the boundaries between rigid-group dynamic domains (Niu et al., 2011). They are also reasonably close to residues implied as dynamic by NMR relaxation exchange ($R_{ex}$) and backbone nuclei exhibiting chemical shift perturbation (Δδ) on addition of substrate (analogs). However, the agreement is better when a stronger $\ell^1$-norm restraint is used instead of stringent subset selection (Figure 2).*

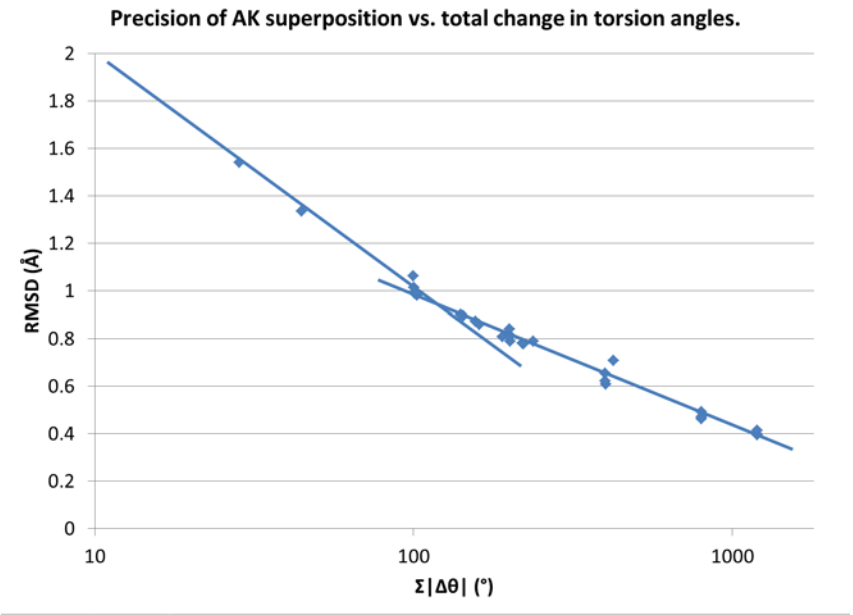


*Figure S3: Precision of superposition depends mostly on the total torsion angle change allowed. The superposition of the AK transition state analog on the substrate-free form was refined thirty times with widely varying parameters (see Experimental Procedures). The target total change in torsion angles, T, was varied between 0 and 1200°, in a modified objective function:* $\sum_{i=1}^{N}\left(\vec{y}_i - \vec{x}_i(\{\Delta\varphi_j, \Delta\psi_j\})\right)^2 + \lambda\left[max\left(\sum_{j=1}^{P}|\Delta\theta_j|\right) - T, 0\right];\ \theta_j = \psi_{j-1} + \varphi_j$. *The $\ell_1$-norm weight, λ, ranged between 0.4 and 1000, while either refining all (φ, ψ) torsion angles or after selecting the 25% most consequential pseudo-dihedrals. The horizontal axis is logarithmic, and there is exponential asymptotic convergence as degrees of freedom are increased. The change in slope occurs approximately at the point where the large scale domain rotations appear mostly complete and further adjustments become more local (Figure S4).*

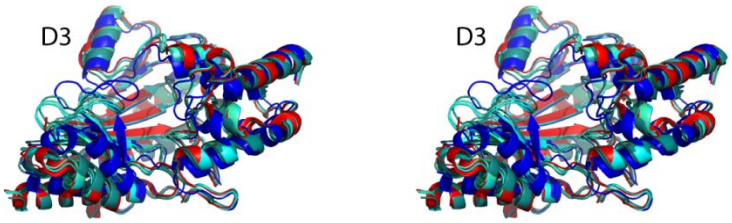


*Figure S4: $\ell^1$-norm restrained refinements with different λ weights. In this stereogram, the AK transition state analog structure (TSA) is shown in blue after rigid superposition on the AK substrate-free structure (red). (φ, ψ)-refinements from the TSA structure towards the substrate-free are shown for λ = (0.4, 5, 50) in cyan in increasingly dark shades, λ = 5 corresponding to figure 2. As the $\ell^1$-restraint is relaxed (decreasing darkness), the structure gets closer to the target (red), starting with the larger subdomains and helices, and ending with finer and more local adjustments. Residual errors are worst at dynamic domain 3 (D3) where the helix motion is shearing (not rotation), accomplished with large counteracting changes to neighboring backbone dihedrals in the adjoining loops. For AK, the transition to more local adjustments occurs with λ between 5 and 2 and corresponds to the change of gradient in Figure S3. Superpositions, optimizing the 25% most consequential dihedrals, give aggregate rotations of 144° and 238° for λ of 5 and 2 respectively.*

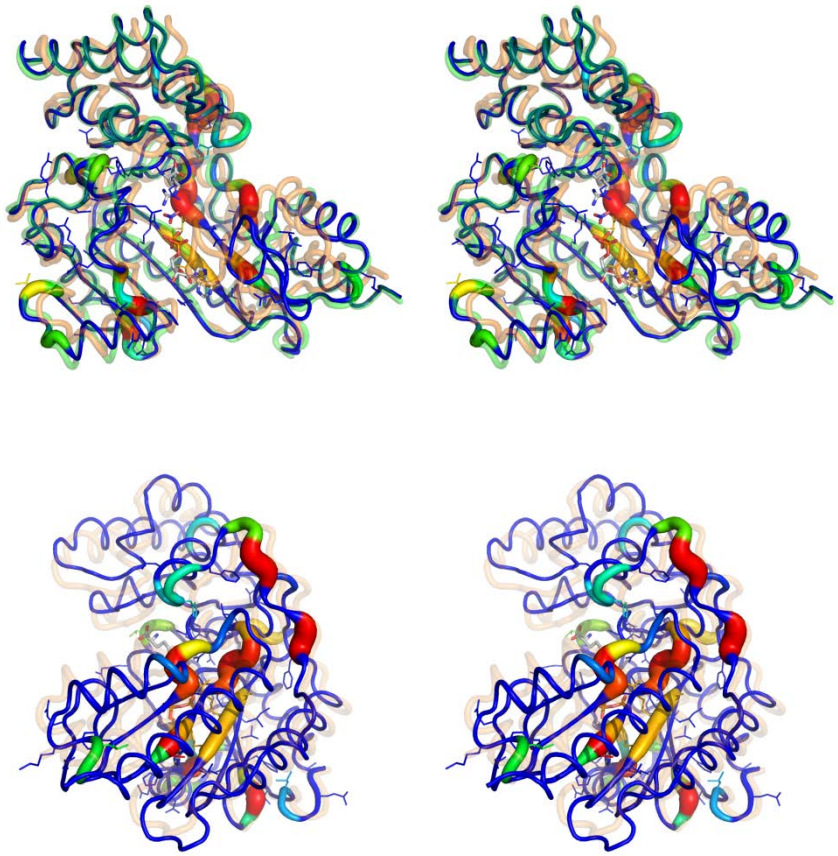

*Figure S5: Stereographic representations of Figure 2B/C. Top (Fig. 2B): Starting from the AK TSA structure (orange), the parsimoniously superposed model (color-coded by pseudo-dihedral rotation, blue to red) is now well fit to the substrate-free form (green). Transition state analogs are shown in stick model. Side chains are shown for residues with backbone nitrogen $R_{ex}$ to highlight proximity to changing dihedrals. Bottom (Fig. 2C): The TSA and superposed structures are rotated 90° to highlight flexing of the β-sheet.*

## Abbreviations

AK: arginine kinase; AdK: adenylate kinase; CS: chemical shift; DHFR: dihydrofolate reductase; NMR: nuclear magnetic resonance; $R_{ex}$: relaxation exchange; RMSD: root mean square deviation; TIM: triose phosphate isomerase; TSA: transition state analog.

## Tables

*Table S1: Typical average pseudo-dihedral differences between related crystal structures (see Figures 3-5). The origins of such differences are not clear, and could result, in part from differences in crystallization (Rashin et al., 2009), or ill-conditioning or over-fitting in structure refinement.*

| Protein | PDB ids | Citations | Resolution | <\|dihedral difference\|> | Comment |
|---|---|---|---|---|---|
| Triose phosphate isomerase (TIM) | 1YPI, 1I45 | (Lolis et al., 1990; Rozovsky et al., 2001) | 1.9 Å | 8 ± 16° | Native vs. mutant |
| RNase A | 2G8Q, 3MZQ | (Berger et al., 2010; Leonidas et al., 2006) | 1.5 Å | 9 ± 23° | Crystal forms |
| Dihydrofolate reductase (DHFR) | 1RG7, 1DDS | (Dunbar et al., 1997; Sawaya and Kraut, 1997) | 2.2 Å | 15 ± 24° | Nominally similar |

*Table S2: Comparison of the 8 most consequential pseudo-torsion angles identified by subset selection with different $\ell^1$ restraint weights (see Experimental Procedures). Reasonable superpositions are achieved with all of these weights (Figure S2). Although neighboring, the exact choice of residues depends on the weighting, exposing ill-conditioning in subset selection and redundancy in dihedral rotations that achieve similar conformational effects.*

| $l^1$-Restraint (sum rotations) | Pseudo-torsion angle residue # (rotation) | | | | | | | | | | | | | | | |
|---|---|---|---|---|---|---|---|---|---|---|---|---|---|---|---|---|
| 0.1 (96.9°) | | 96 | 98 | | 102 | | 127 | | 135 | 213 | | | 281 | | 284 | |
| | | (11.6°) | (-12.2°) | | (-14.7°) | | (-16.6°) | | (-4°) | (-8.7°) | | | (-18.6°) | | (-10.5°) | |
| 0.4 (102.2°) | | 96 | 98 | | 102 | 125 | | 132 | | 213 | | | | 283 | | 323 |
| | | (12°) | (-11.9°) | | (-14.4°) | (-8.5°) | | (-8.6°) | | (-8.7°) | | | | (-23.9°) | | (-11.4°) |
| 2 (73.2°) | | 96 | 98 | | 102 | | 127 | | | | 277 | 279 | | 283 | 284 | |
| | | (12.7°) | (-12.5°) | | (-10.5°) | | (-10.2°) | | | | (-9°) | (-3.3°) | | (-8.4°) | (-6.6°) | |
| 10 (74.7°) | 92 | | 98 | 100 | 102 | 125 | | | | | 277 | | | 283 | 284 | |
| | (8.3°) | | (-11.8°) | (6.9°) | (-7.1°) | (-12.7°) | | | | | (-9°) | | | (-10.5°) | (-8.4°) | |
| Region | I | | | | | II | | | | III | IV | | | | | V |

*Table S3: Superposition of AK TSA on substrate-free form, dependence of RMSD on the weight, λ, of the $\ell^1$ –norm (T=0, subset of 25% highest impact pseudo-dihedrals; see Figures 2 & S4).*

| λ weight | ∞* | 50 | 10 | 5 | 2 | 0.4 |
|---|---|---|---|---|---|---|
| RMSD | 3.10 Å | 1.34 Å | 0.99 Å | 0.89 Å | 0.79 Å | 0.71 Å |
| $\sum_{j=1}^{P}\lvert\Delta\theta_j\rvert$ | 0° | 45° | 101° | 144° | 238° | 423° |

* i.e. rigid superposition without torsion angle refinement.

*Table S4: Largest hinged rotations between the substrate-free and transition state analog complex of arginine kinase (see Figure 2).*

| Hinge | Residues | Rotation | Comment |
|---|---|---|---|
| Domain linker | 90-102 | 20.2° | Consistent with DynDom analysis showing 21.2° rotation between dynamic domains 1 and 4 (Niu et al., 2011) |
| Nr. β-strand 6 | 277-9 / 283-4 | 18.6° | Corresponding rotations throughout the sheet, in adjacent strands β5 and after β7. |
| β-strand 5 | 125-7 | 10.7° | Part of the β-sheet twisting, see above. |
| Post-β-strand 7 | 328-31 | 9.9° | Part of the β-sheet twisting, see above. |
| Pre-α-helix 12 | 171-6 | 7.4° | Loop at N-terminal end of moving helix. |
| Post-α-helix 12 | 187-8 | 7.5° | Loop at C-terminal end of moving helix. |
| Adjacent loops | 135, 198 | 5.2°, 4.2° | Near interface between N- and C-domains. |
| β-strand 2 | 213-4 | 6.1° | Same β-sheet as strands 5, 6 & 7 (above), but opposite side. |

## Experimental Procedures

In developing robust computer methods for superimposing protein structures with minimal (parsimonious) changes in the backbone dihedral angles, a number of algorithms were evaluated, not only for their numerical properties (conditioning and convergence), but also for consistency of the output with experimental data. Both in algorithm selection, and also in the selection of optimal running parameters, arginine kinase (AK) was the prime test system. The Supplementary Experimental Procedures describes the process by which the algorithms were chosen for the methods described in the main paper, the optimization of algorithmic parameters, cross-checking of the output in a number of ways, and defining the limits of the algorithms.

### Convergence tests

Flexible least-squares superposition through refinement of internal coordinates was expected to be a highly non-linear optimization. Convergence was tested on AK when optimizing only backbone φ and ψ (other geometries fixed), and without added restraints. Exhaustive refinement yielded a backbone/$C_\beta$ RMSD of 0.37 Å, judged to have converged within experimental accuracy, given that the A and B subunits of substrate-free AK also differ by 0.37 Å. RMSD is not expected to reach zero, crystallographic refinements yielding differences in peptide ω torsion angles and deviations from ideal stereochemistry that are not addressed in φ,ψ-optimization. Absent restraint, refinement changed the dihedrals much more ($\sum_i \Delta|\theta_i| = 1706°$) than the expected 247° needed to rotate *quasi*-rigid fragments. When examined locally, the poorest superimposition was near dynamic domain 3 (Niu et al., 2011) where adjacent residues show large (Δφ, Δψ) differences, up to = -153°, 120° for $Gly_{191}$ as an α-helix is translated 3 Å in a shearing motion. Our global optimization using internal coordinates is least effective at resolving modest motions resulting from large torsional rotations that are mostly offsetting. For AK, this affects one 21-residue region in a 359-residue protein.

**Subset selection**

Elimination of parameters by subset selection led to computational efficiencies and insights into the redundancy of conformational change, but not to an improvement in the quality of superposition. The goal in subset selection was reduction in degrees of freedom with minimal degradation of the RMSD. Exhaustive combinatorial search for the best subset of torsion angles to vary was computationally intractable. Instead, dihedrals deemed to be of least impact were pruned iteratively, fixing them at starting values. Ranking was greatly complicated by the interdependence of dihedral parameters. Estimates from the first order partial residual derivatives, $\left\{\frac{\partial O}{\partial \theta_j}\right\}$, for the objective function, $O = \sum_i \left|\overrightarrow{x_i} - \overrightarrow{x_{0,i}}\right|$, for starting structure, $x_{0,i}$, proved to be poor proxies for impact in AK. Better was a ranking calculated from the steepest descent shift vectors summed over *C* cycles of refinement, $\left\{\sum_{c=1}^{C} \frac{\partial O_c}{\Delta O_c \cdot \partial \theta_j}\right\}$. Better still (50% lower RMSD), was a ranking by rotation size in a prior $\ell^1$-restrained refinement. This works, because: (1) an $\ell^1$-Norm dampens changes in less impactful parameters; and (2) the BFGS optimizers (Nocedal, 1980; Nocedal and Wright, 2006) use an approximation to the Hessian matrix for direction vectors, thereby capturing parameter interdependence through second order partial derivatives. Each iteration consisted of: 20 cycles of $\ell^1$-Norm restrained refinement from which a (small) fraction of the remaining parameters of least consequence would be fixed; and 20 cycles of unrestrained optimization with the remaining dihedrals from which statistics would be calculated. Pruning to the top 10% was achieved in 3 iterations, then from the top 30, *pseudo*-dihedrals were pruned one per iteration (down to 1) in the hope of robustly identifying the most consequential dihedrals. With a wide range of $\ell^1$-penalties (λ), fixing 75% of the dihedrals improves the RMSD (Figure S2A), then as the number is culled down to 7-14 torsion angles (depending on the λ restraint weight), RMSDs gradually worsen. With further subset selection, the deterioration is more marked (at all λ), indicating that a minimum of about 10 dihedrals is

required to model the principal changes. As the number of variable dihedrals increases from ~10 to 100, the decrease in RMSD likely reflects both real improvement and over-fitting. The total change ($\sum|\Delta\theta|$) rises near linearly with the number of variables, even as gains in RMSD diminish (Figure S2B). Furthermore, λ can be chosen such that the $\ell^1$-Norm reduces $\sum|\Delta\theta|$ without affecting the RMSD (Figure S2C). Remarkably, a reasonable approximation to the overall conformational change can be achieved by varying just 8 or 2% of the *pseudo*-torsion angles (Figure S2). With only 8 *pseudo*-torsion angles, 20 cycles was sufficient for full convergence, but the RMSD remains substantially inferior to refinement that is LASSO-restrained, but otherwise unconstrained.

Detailed analysis of subset selection offers insight into determinacy of the computation and redundancy in the mechanics of conformational change. Table S2 shows the commonalities and differences in selected subsets when pruned aggressively using different $\ell^1$-weights. The three regions with largest dihedral rotations (I, IV & II, respectively) dominate irrespective of $\ell^1$-weight, with two smaller rotations (V & III) present only with weaker restraint. The exact composition of each region depends somewhat on the restraint. Region I contains a common core of residues, but one rotation is shifted 4 amino acids at high λ. Likewise, there is variation in the identity of the first residue in region IV. Finally, the total rotation in region III of 20° or 11° depends on whether a compensating 9° rotation has been selected at residue 213 (region III). Regions I through V correspond to multi-residue "hinge" segments of high torsion angle change in the refinement of Figure S1B. Stringent selection forces rotations to be concentrated within a small subset of hinge residues. The dependence of exact residue identities on λ indicates poor conditioning, highlighted when subset selection is pushed to this extreme (8 residues). It also shows selection bias, a common artifact of subset selection algorithms (Tibshirani, 2011), in which the final solution depends arbitrarily on earlier poorly conditioned decisions. Thus, while

subset selection is robust in terms of approximate locations of key rotations, at a detailed level, it is possible for subset selection to return slightly different combinations of residues whose rotations yield similar overall structural transitions. Stringent subset selection is not reliably narrowing down to key rotations with amino acid accuracy. In fact the diversity among the solutions suggests that none of the heavily pruned subsets is a better representation of reality than the more dispersed hinge rotations that emerge with $\ell^1$-restraint alone.

While an $\ell^1$-restrained model might be a more faithful representation, subset selection shows that a very low parameter model that is stereochemically plausible can be a reasonable approximation, should it be needed in fitting very sparse experimental data. Such models might not be unique representations down to amino acid level, but rotations are being made at sites approximately consistent with the other available evidence: close to boundaries between rigid-group dynamic domains (Niu et al., 2011), or residues exhibiting backbone dynamics through NMR relaxation exchange (Davulcu et al., 2009), or residues exhibiting chemical shift perturbation on addition of substrate (analogs). Finally, the poor conditioning in subset selection reminds us that, at a mechanical level, a protein carries redundancy in exactly which of neighboring residues undergo dihedral rotations to achieve a large-scale domain rotation.

Subset selection is better conditioned when pruning is less aggressive. When stopping with the highest impact 30 dihedrals, rotations selected using $\lambda = 10$ correlate well ($r = 0.96$) with those selected using $\lambda = 2$. Twenty cycles of refinement proved sufficient for robust filtering out dihedrals of negligible consequence. As the computation of superposition depends linearly on the number of dihedrals, efficiency could be improved with 20-cycle batches to fix 50%, then 75% of the least-impactful. Subsequent exhaustive $\ell^1$-restraint refinement of the remaining 25% yielded results similar to refinement with all dihedrals variable, but in one quarter of the time.

With such pre-filtering, subset selection is used for efficiency, but it is the $\ell^1$-Norm in the final batch that is enforcing parsimony.

**Restraining or constraining the total dihedral change with subset selection and the $\ell^1$-norm.**

Optimization can be run in several ways, optionally selecting out inconsequential parameters, and with different choices for the $\ell^1$-Norm weight, λ, with or without some target total of rotations, T (Figure S3). Together they control the total change, $\sum_{j=1}^{P}|\Delta\theta_j|$, on which the precision of superposition primarily depends (Figure S3). The solution depends little on whether dihedral changes are restrained from the start (T = 0), or, to improve convergence rate, only after reaching a T > 0 threshold, when it can be enforced as a *pseudo*-constraint using a high λ. For simplicity, in other parts of the paper, T = 0, so that λ is the only user-controlled parameter.

**Do NMR $R_{ex}$ locate hinges more accurately than our computational analysis of structures?**

Flexible parsimonious superposition identifies hinges with an accuracy of a few residues. Does the experimental NMR $R_{ex}$ do better than the computational analysis? Refining the *pseudo*-dihedrals in AK just for residues with $R_{ex}$ (λ = 5) gives an RMSD of 1.15Å, somewhat inferior to the 0.89Å of unconstrained superimposition. Rotation in the flexible linker is only 10.6°, but increases to 22.5° if rotations in residues 98 to 102 are also permitted, reducing the RMSD to 1.0Å, still inferior. This supports the view that much of the difference between the superposition and the NMR data arises because dynamics are not observable through $R_{ex}$ in a few locations.

**Rationalization of AK NMR $R_{ex}$ by proximity to hinges and other structural changes.**

In the main paper, computational inference of flexible *pseudo*-dihedrals is validated by comparison to measured $R_{ex}$ or Δδ. Here, the comparison is inverted, starting with the observation that residues with significant $R_{ex}$ or Δδ are, on average 2.2 residues from any of the top 50 *pseudo*-dihedral rotations. As noted earlier, chemical shift that underlies both $R_{ex}$ and δ

measurements can be perturbed indirectly through changes to the atomic environment. The crystal structures were examined to see if any of $R_{ex}$ and Δδ more likely resulted from changes in through-space interactions in which backbone changes in one region could have impact at sites remote in sequence number. There are 23 residues with $R_{ex}$ in substrate-free AK which do not agree on a one-to-one basis with hinges identified through parsimonious superposition. These residues lie in either an active site loop (I182, D183, D184, H185, E190, G191, D192, R193, T197, A200, C201, R202, T206, R208, and G209) or at the interface between the N- and C-terminal domains of the enzyme (D71, F136, N137, F270, C271, N274, G276, and G332). As discussed previously, the precision of our hinge identification is about ±3 residues, within which 75% of the latter interface residues fall, as do three residues in the loop (T197, A200, and C201). As for the remaining loop residues, E190-R193 exhibit the largest of all *pseudo*-dihedral differences between the substrate-free and TSA bound AK (73° to 153°), so large local backbone changes might account for intrinsic $R_{ex}$. Residues I182-H185 lie in the α-helix preceding the loop that, on substrate-binding, is translated across the active site and rotated about the helix axis. I182 moves 2Å closer to L187 and loses solvent exposure. H185 undergoes a 25° change in *pseudo*-dihedral, but, with its large translation, its backbone nitrogen comes 4Å closer to M233, and its side chain is brought from 13Å to within 4Å of H284. If the intrinsic motions mimic, in part, those associated with substrate-binding, $R_{ex}$ of these residues can be rationalized. In summary, there is good agreement between $R_{ex}$ and the hinges derived in our analysis of structure, with most of the additional $R_{ex}$ at sites either of changed loop conformation or affected substantially by through-space changes.

**NMR relaxation dispersion analysis for the AK TSA complex**

$^{15}N/^{2}H$-enriched arginine kinase was prepared as previously described. The transition state analog complex was formed by exchanging purified enzyme into a solution of 10 mM D4-

imidazole (pH = 6.5), 1.0 mM dithiothreitol, 200 μM $NaN_3$, 6 mM ADP, 8 mM $MgCl_2$, 60 mM arginine, 20 mM $NaNO_3$, 90% $H_2O$, and 10% $^2H_2O$. TSA components ADP, arginine, and $NaNO_3$ were present 40- to 60-fold higher than their respective $K_D$'s thus ensuring AK was >98% saturated. Backbone resonance assignments for arginine kinase in the TSA complex have been reported (Davulcu et al., 2013).

NMR data were recorded at 25 °C on a Varian INOVA 600 NMR spectrometer equipped with a cryogenic HCN probe, processed with FELIX 2007 (FELIX NMR), and analyzed using Sparky 3 as previously described (Davulcu et al., 2009; Goddard and Kneller, 2004). $R_{ex}$ was quantified using a constant-time $^{15}N$ CPMG relaxation dispersion experiment with TROSY detection (Loria et al., 1999). A constant relaxation time of 32 milliseconds and CPMG effective field strengths of 31.25*, 62.5, 93.75*, 125, 187.5, 250, 500, 750, and 1000 Hz were employed. Asterisks denote points which were measured in duplicate for error estimation. $R_2^{eff}$ was determined using a two-point function: $R_2^{eff} = \left(-\frac{1}{\tau_{relax}}\right)\ln(\frac{I_\nu}{I_0})$, where $\tau_{relax}$ is the relaxation time, $I_\nu$ is the intensity of a given resonance at a CPMG effective field strength, and $I_0$ is the intensity of the resonance in the reference measurement omitting the CPMG block. $R_{ex}$ is the difference of $R_2^{eff}$ (v = 0 Hz) and the intrinsic relaxation rate constant $R_2^0$.

**Possible extensions of the computational analysis**

The current implementation can be extended in several ways. Restraints on the values of dihedrals are possible, but have not been a priority, because rotations are mostly small and within the favored regions of a Ramachandran plot. Rotations about the peptide ω are not allowed, but ϕ & ψ rotations are sometimes no larger than common distortions of ω, so this could be revisited. Finally, different λ parsimony restraints can be optimal for different regions of

a structure.  This would be a trivial extension, but we have opted for a uniform λ for each run, so that superposition depends on just one user-adjustable parameter.

## References


Berger, M.A., Decker, J.H., and Mathews, II. (2010). Diffraction study of protein crystals grown in cryoloops and micromounts. J Appl Crystallogr *43*, 1513-1518.

Davulcu, O., Flynn, P.F., Chapman, M.S., and Skalicky, J.J. (2009). Intrinsic domain and loop dynamics commensurate with catalytic turnover in an induced-fit enzyme. Structure *17*, 1356-1367.

Davulcu, O., Niu, X., Brüschweiler-Li, L., Brüschweiler, R., Skalicky, J.J., and Chapman, M.S. (2013). Backbone resonance assignments of the 42 kDa enzyme arginine kinase in the transition state analogue form. Biomolecular NMR Assignments, 1-4.

Dunbar, J., Yennawar, H.P., Banerjee, S., Luo, J., and Farber, G.K. (1997). The effect of denaturants on protein structure. Protein Science *6*, 1727-1733.

Goddard, T.D., and Kneller, D.G. (2004). SPARKY 3. (University of California, San Francisco).

Hayward, S., and Lee, R.A. (2002). Improvements in the analysis of domain motions in proteins from conformational change: DynDom version 1.50. J Mol Graph Model *21*, 181-183.

Leonidas, D.D., Maiti, T.K., Samanta, A., Dasgupta, S., Pathak, T., Zographos, S.E., and Oikonomakos, N.G. (2006). The binding of 3'-N-piperidine-4-carboxyl-3'-deoxy-ara-uridine to ribonuclease A in the crystal. Bioorg Med Chem *14*, 6055-6064.

Lolis, E., Alber, T., Davenport, R.C., Rose, D., Hartman, F.C., and Petsko, G.A. (1990). Structure of yeast triosephosphate isomerase at 1.9-A resolution. Biochemistry *29*, 6609-6618.

Loria, J.P., Rance, M., and Palmer, A.G., 3rd. (1999). A TROSY CPMG sequence for characterizing chemical exchange in large proteins. J Biomol NMR *15*, 151-155.

Niu, X., Bruschweiler-Li, L., Davulcu, O., Skalicky, J.J., Bruschweiler, R., and Chapman, M.S. (2011). Arginine Kinase: Joint Crystallographic and NMR RDC Analyses Link Substrate-Associated Motions to Intrinsic Flexibility. J Mol Biol *405*, 479-496.

Nocedal, J. (1980). Updating Quasi-Newton Matrices with Limited Storage. Mathematics of Computation *35*, 773-782.

Nocedal, J., and Wright, S.J. (2006). Numerical optimization, 2nd edn (New York: Springer).

Rashin, A.A., Rashin, A.H., and Jernigan, R.L. (2009). Protein flexibility: coordinate uncertainties and interpretation of structural differences. Acta Crystallogr D Biol Crystallogr *65*, 1140-1161.

Rozovsky, S., Jogl, G., Tong, L., and McDermott, A.E. (2001). Solution-state nmr investigations of triosephosphate isomerase active site loop motion: ligand release in relation to active site loop dynamics. J Mol Biol *310*, 271-280.

Sawaya, M.R., and Kraut, J. (1997). Loop and subdomain movements in the mechanism of Escherichia coli dihydrofolate reductase: crystallographic evidence. Biochemistry *36*, 586-603.

Tibshirani, R. (2011). Regression shrinkage and selection via the lasso: a retrospective. Journal of the Royal Statistical Society B *73*, 273-283.